Original article

JOURNAL OF
REINFORCED
PLASTICS &
COMPOSITES

A study of the interactions of carbon based fillers in acrylonitrile butadiene rubber matrix for high deformation sensor applications

Journal of Reinforced Plastics and Composites
2023, Vol. 0(0) 1–16

DOI: 10.1177/07316844221145644
journals.sagepub.com/home/jrp
SAGE

Bismark Mensah, Abu Yaya, Boateng Onwona-Agyeman,
Ralph Abakah Ofori and Clive Dompreh

Abstract

A strain sensor was prepared by reinforcing acrylonitrile butadiene rubber (NBR)-5 parts per hundred of rubber (phr) carbon black (CB_H) separately with small concentration (~0.1phr) of reduced graphene oxide (G_L), multi-walled, and carbon nanotube (NT_L) via a combination of conventional solution and solid processing techniques. The interactions and the electronic properties among carbon based fillers NT, CB, G and their synergy effects (NBR-CB_H-G_L and NBR-CB_H-NT_L) were investigated by using density functional theory (DFT) modeling approach. The DFT predictions were in correspondence with the experimental results. The optimum design (NBR-CB_H-G_L) was found to show high curing, mechanical and improved electrical properties. On account of strain sensing performance, NBR-CB_H-G_L exhibited high gauge factor (GF) $\sim 10^5$ at 0–40% strain, which was over 900% than NBR-CB_H (GF $\sim 10^4$ at 0–30% strain) and the highest reported so far. This was explained by the breaking of CB networks caused by tight NBR-G structures on straining, leading to high electrical resistance. The NBR-CB_H-G_L also demonstrated high stability and repeatability in the cyclic loading. In terms of applications, NBR-CB_H-G_L exhibited high capability for vibration detections and wearable sensing, especially for detection of human bodily motions like speeches, facial deformations, bending, and relaxation of the fingers.

Keywords
Sensor, carbon nanotubes, graphene, carbon black, gage factor and acrylonitrile butadiene rubber, DFT modeling

Introduction

Conventional metallic strain sensors are not useful where high deformations above ~5% strain are required. This has led to pursue of other materials such as polymer-based sensors, which are suitable for such a large deformation sensing. A number of polymer-based sensors based on conducting particles like carbon nanotubes (NT), carbon black (CB), and nanofibers etc. are proposed.[1–8] Recently, Wenjun and co-workers [2] fabricated an elastomer bilayer material based on highly NT-loaded polydimethlysiloxane (PDMS) for a force sensor. This showed a stretchability in the range of 2.6~14% with desired electrical response as a sensor. A similar study with NT-filled polymer nanocomposite is extended on by Yin et al.,[1] Loh et al.,[3] and Xu et al.[2] The works of Dai group,[9] Hu et al.,[10] Luheng and Wang group,[4,5] and Shuai Chen et al.,[11] are all interesting literature on polymer-based strain sensor that make use of single fillers like NTs, CB, and graphenes (G) particles.[3,9,12–16] The gage factor (GF) is one of the important parameters for qualifying the performance of sensors and it is defined as[1–5]

$$GF = \frac{\Delta R / R_0}{\varepsilon} \tag{1}$$

where R_0 is the initial resistance, ΔR is the difference of resistance during deformation, and ε is the strain. Most of polymer-based strain sensors demonstrate high deformation capability, and they're under vigorous studies with conductive fillers to develop sensors with high electrical sensitivity performances compared with conventional metallic strain gages whose GF values of ~2(1–5). So far, the polymer-based strain sensors with single filler systems have

---

Department of Materials Science and Engineering, CBAS, University of Ghana, Legon, Ghana

Corresponding author:
Bismark Mensah, Material Science and Engineering, University of Ghana College of Basic and Applied Sciences, P.O.BOX LG 77 Legon, Accra 0233, Ghana.
Email: bismarkmensah@ug.edu.gh

been reported to show GF values of ∼0.06–350, with a strain up to ∼800%.[3,9,12–15]

In recent times, the use of the mixtures of single fillers systems like carbon based fillers like CB/G(18–20), CB/NT(21, 22), G/NT(23, 24) into/onto polymer matrices for the fabrication of polymer based materials for advanced applications including strain sensor, is currently receiving greater attention as an alternative way to improve the GF of polymer-based strain sensors. Kurian et al.[17] earlier explored the use of complementary behavior of CB/G in PDMS to prepare sensor with stretchability up to 300%, and the gauge factor (GF) depended on the composition of the composites. Song et al.[18] recently conducted a similar study of PDMS-CB-G composites with gauge factor of ∼1.9×10^4 within 28–44% strain. Highly stretchable PDMS-G-NT fibers were successfully prepared via a facile direct ink writing technique and recorded GF of ∼1.5×10^4 at an improved strain 100% strain.[19] By considering the cost of G and NT, blending the two (G/NT) might increase the cost of such designs as far scalability is concerned. Even though, the studies involving dual filler systems in or onto polymer matrix for sensors generally show high GF and stretchability over the single filled polymer composites systems, but they do not clearly explained the mechanisms that leads to such enhancements in electrical conductivity and consequently the high GF of the corresponding sensors. Instead, these studies have only reported scattered results leading to low percolation threshold they observed for these synergy filler systems.[17,18,20] Therefore, further works will be needed to understand dual filler interactions in polymer matrix, in order to further improve the stretchability and the GF of dual filler systems embedded or coted onto polymer matrix systems. The purpose of this present work is to investigate the electrical conductivity performance of mechanism of dual filler systems in acrylonitrile-butadiene rubber (NBR) matrix using theoretical modeling and experimental works and their potential applications for strain sensors.[21,22,23] First, a computational tool was used to predict the electronic properties of single (G, CB, and NT) and the dual (CB-G and CB-NT) filler systems in NBR matrix. In the experimental work, the three carbon-based conducting fillers of CB, NT, and graphene (G) were incorporated separately into NBR by a combination of solvent and melt mixing technique. Later, small amount (0.1 phr) of relatively expensive filler like G or NT were incorporate into a 5 phr of cheaper conductive CB filler and the synergistic effect among fillers, CB-G and CB-NT were studied. The physical properties, notably cure and tensile, were measured. The electrical properties including GF were monitored as a function of uniaxial strain. The NBR-CB_H-G_L composition was observed to be the best candidate of sensing material and some experimental set up was made to check the possibility of using it as a wearable and stretchable device for monitoring the dynamic, weighing, and human body deformation sensing behavior.

Experimental

Materials

An acrylonitrile-butadiene rubber (NBR, KNB 25LM™, acrylonitrile content: 20–30%, Kumho Petrochemical Co. Korea) was used as a base rubber. Three types of conducting fillers were employed in this study. They were graphene (G; particle size: ∼78 nm, thickness: 0.8∼2 nm, prepared in our lab.),[24] carbon black (CB; Ketjen™ black EC600JD, weak pellet type: 3 mm particle diameter, Brunauer–Emmett–Teller (BET) surface area: ∼1400 m^2/g, pore volume: 480∼510 mL/100 g, Akzo Chem), and carbon nanotube (CNT; Hollow CNT75LD, purity: 95%, OD: <2 nm, Length: 5–30 μm, NanoKarbon Co.,Ltd., Korea). The remaining ingredients were used as the typical grades in rubber industries. The compound formulation and designation is presented in Table 1.

Theoretical predictions: computational modeling

The models, which include Acrylonitrile butadiene rubber (NBR), Reduced Graphene oxide (G), pure graphene (GR), Carbon Black (CB), and Multi-walled Carbon Nanotubes (NT), were constructed using the Avogadro software, by specifying the structure of the models and atomic positions. These models were saved under protein data bank file extensions and exported to materials studio software for further calculations. Adsorption models were created using the adsorption module locator and the following interactions were achieved: NBR, NBR-CB, NBR-G, NBR-NT, NBR-CB-G, and NBR-CB-NT. These interactions were achieved under simulated annealing conditions with fine quality. The loading was set to one [1] and the properties were set to low energy configurations under the property tab with the fixed number of configurations set to 10. The most stable interaction was determined by the complex with the lowest energy value. The next stage was to geometrically optimize the structures (relax) together with Self-Consistent Field (SCF) calculations, since the models built by Avogadro were not in their lowest state. Under geometry optimization, each of the atoms was moved around in space until a coordinate was found where the net interatomic force between the atoms was zero or close to zero. This was done because in Density Functional Theory (DFT), calculations are more accurate for ground states than excited states. This was achieved using the calculation tool in Materials Studio. In the calculation tab, the task was set to geometry optimization and the function was set to Generalized Gradient Approximation together with Perdew, Burke and Ernzerhof (PBE) approaches. The maximum optimization and SCF cycles were set to 1000 iterations, and a smearing value of 0.5 Hartree was used to perform the calculations. Density of states analysis was added to optimization calculations in the properties tab with the number of bands set to 20. The calculation was run on four cores of the CPU. The average optimization step was found to be after 200 cycles. After the calculations were run, the optimized

Table 1. Composition of NBR filled with various carbon based particles and their codes.

Compound	NBR	NBR-G_L	NBR-G_H	NBR-NT_H	NBR-CB_H	NBR-CB/NT_L	NBR-CB/G_L
NBR	100	100	100	100	100	100	100
G	—	0.1	5.0	—	0.1	—	0.1
NT	—	—	—	5.0	—	0.1	—
CB	—	—	—	—	5	5.0	5.0
ZnO	5	5	5	5	5	5	5
SA	1.5	1.5	1.5	1.5	1.5	1.5	1.5
CZ	0.5	0.5	0.5	0.5	0.5	0.5	0.5
TMTD	0.25	0.25	0.25	0.25	0.25	0.25	0.25
S	2	2	2	2	2	2	2

G: graphene, NT: carbon nanotube, CB: carbon black, ZnO: zinc oxide, SA: stearic acid, CZ: N-cyclohexyl-2-benzothiazolesulfenamide, TMTD: tetradimethylthiuram disulfide, S: sulfur.

structures were generated together with an output script containing the binding energies after convergence together with HOMO and LUMO energies from which the band gap was calculated by the relation EG = $E_{LUMO} - E_{HOMO}$ where EG is the band gap energy. The densities of states plot were generated from the optimized molecules.

Practical approach

Preparation of nanocomposites. The preparation of all the specimens follows the same procedure used in earlier by Mensah et al. work[25] except for the dual filler preparation. In this case, the G, CB, NT, CB-G, and CB-NT particles were separately dispersed in dimethylformamide (DMF) under ultrasonication for 2 h. Later, the mixtures of the single fillers and the dual CB_H-G_L and CB_H-NT_L blends were then introduced separately into the NBR dissolved in acetone, and they were coagulated by adding de-ionized water. The coagulated rubber composites (NBR-G_L, NBR-G_H, NBR-NT_L, NBR-CB_H, NBR-CB_H-NT_L, and NBR-CB_H-G_L) were dried in an oven at 80°C. The sulfur curing additives (ZnO, TMTD, SA, CZ, and S) were dispersed in the prepared composite using a two-roll mill (Mixing Roll M/C, Model: DS-1500R, WITH LAB. Co. Ltd) and then sheeted out. The NBR nanocomposites were cured for the optimum cure condition by a hot press machine (Caver WMV50H, USA) at a pressure of ~11 MPa and at 160°C. The samples were cut into standard shapes of dumbbell shape for tensile test, square shape for swelling test, and rectangular shape for sensing and electrical property tests.

Characterization

Cure property. The cure property was measured at 160°C by a cure rheometer (ODR 2000, Alpha Technologies, USA). The cure properties including onset of cure time (t_{s2}), optimum cure time (t_{90}), cure rate index (CRI = $100/(t_{90} - t_{s2})$), maximum (M_H) and minimum torque (M_L), and change in torque ($\Delta M = M_H - M_L$) were obtained.

Crosslinking density. The crosslinking density was performed by swelling NBR composites in methyl ethly ketone (MEK) (molar volume of 89.6 mL/mol) for ~72 h at room temperature. Full detail of the swelling experiment has been reported in earlier by Mensah et al.[25] The liquid absorbed ($W_s - W_i$) and the dried weights (W_{dr}) of the samples were used to calculate the degree of swelling (Q_r) by using the equation below

$$Q_r = (W_s - W_i)/W_{dr} \tag{2}$$

The crosslinking density n_c (mol/cm^3) of the samples were calculated by employing the Flory–Rehner model[26] as shown below

$$n_c = -\left[\ln(1 - v_2) + v_2 + \chi_1 v_2{}^2\right] \Big/ v_1 \left(v_2^{1/3} - v_2 \Big/ 2\right) \tag{3}$$

where the v_2 is the volume fraction of the polymer in a swollen gel at equilibrium given by ($1/Q_r$). v_1 is the molar volume of MEK. With the help of the molar v_1 of the solutions, and the solubility parameter of NBR (8.9 (cal/cc) $^{1/2}$), MEK (9.27 (cal/cc)$^{1/2}$), the interaction parameters (χ_1) between NBR and MEK were calculated to be 0.384 by using the Bristow–Watson equation;[27]

$$\chi_1 = \beta_1 + (v_1/RT)\left(\delta_s - \delta_p\right)^2 \tag{4}$$

where R, T, β, and δ are the universal gas constant (8.314 J/mol.K), absolute temperature, lattice constant (usually about 0.34), and solubility parameter (subscript s and p represent solvent and polymer, respectively).

Tensile strength. The tensile properties were measured at room temperature by using (Lloyd Instrument, UK) with dumbbell shaped specimen (ASTM D412). The cross-head speed was 500 mm/min. The elongation at break E_{br}(%) and tensile strength TS(MPa) were deduced from the stress-strain curves. At least four samples were tested for each composition and averaged.

Electrical resistance. The electrical resistance of each compound with dimension (width: 15 mm and thickness: ~1 mm) was measured by a high-resistance meter (Keithley

Figure 1. Experimental set-up for some applications: (a) dynamic cyclic test (b) sensor placed at the throat, and (c) sensor placed in-between upper lip and the nose.

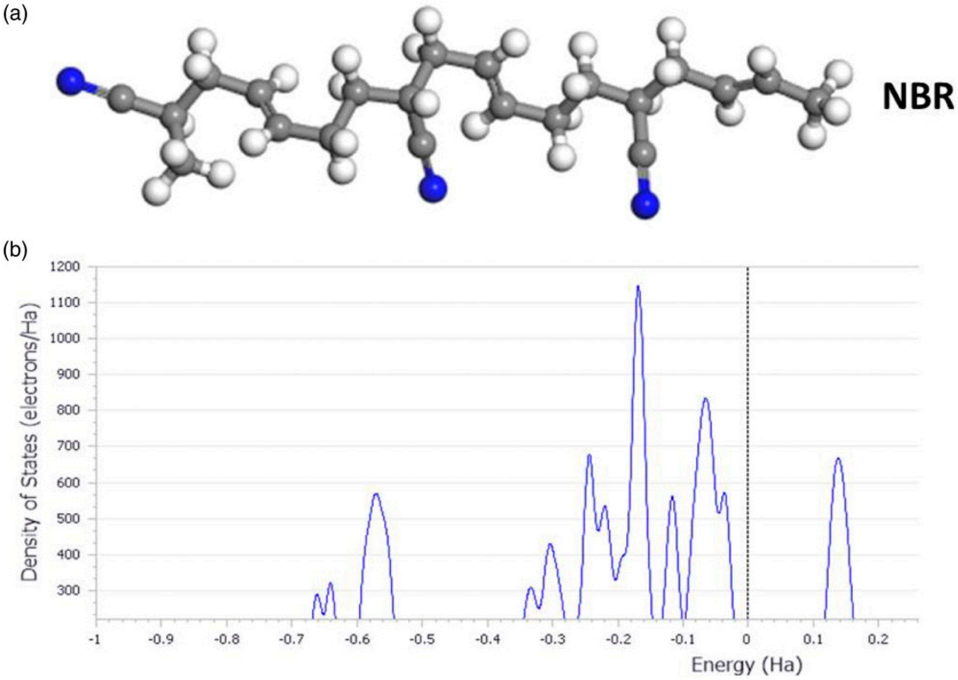

Figure 2. Showing (a) optimized NBR and (b) DOS for NBR.

Electrometer 6517B) at room temperature. The distance between the applied positive and negative electrodes was about 5 mm. The time allowed for measuring was 1.5 min. To check the effect of strain, the sample was uniaxially strained by a precise caliper ruler to the desired strain level, and the resistance was measured. The electrical resistance was also monitored in real time during a dynamic cyclic deformation for 2000 cycles at room temperature (Figure 1(a)). The dynamic amplitude was set to 10 and 30% strains optimum and at a frequency of 2.5 Hz. An experimental set-up was done for the optimum sensor for any possibilities of sensing applications which involves sensing of vibrations or signals from the human body deformations. The sensor involves a rectangular thin film (dimension: 39 × 11 × 0.4 mm) mounted on a wearable silicone rubber of thickness ~1.85 mm. The prepared sensor system was loosely attached to various parts of human body including throat (Figure 1(b)), in-between mouth and nostril (Figure 1(c)) and the fingers, where the skin deformation and vibration was noticeable. The change in the electrical resistance was carefully monitored depending on various body actions like breathing, making the sound "whooo," talking, smiling, and bending and relaxation of the fingers.

Results and discussion

Computational modeling-a DFT approach

NBR and NBR-CB system. The Figure 2(a) represents the optimized structure while Figure 2(b) represents density of states (DOS) plot of the NBR. The average bond length for the optimized structure was found to be 1.232 Å.

The DOS plot for the pristine NBR shows that there are no states existing around and across the Fermi energy level, indicating that the material behaved as an insulator with a wide bandgap of 7.638 ev. This agrees well with experimental result reported for most insulating elastomers.[28] The most stable interactions of NBR with CB can be seen in Figure 3(a) with an average bond length of 1.005 Å. These interactions decreased the band gap by 51% to 3.775 ev. This decrease in band gap accounted for increase in conductivity of the NBR hence its semi-conductive properties which are evident by the DOS plots in Figure 3(b) and this agrees with experimental conclusions.[28] A binding energy of 864.2 ev was recorded, which accounts for moderate intermolecular interactions upon adsorption.

Interactions of CB-G in NBR. Figure 4(a) represents the optimized geometry of the only G and the optimized structure of interactions between G and CB. Pure or defect-free graphene has band gap of ~0.07 ev,[29–31] upon oxidation and reduction to G, it band gap increases to 1.193 ev, though still electrically conductive, as reported by Abid et al.[29] The interaction of G with CB increased the conductivity of the CB by 6% to a value of 1.125 ev. The DOS plot in Figure 4(b) also confirms that the material possesses conductive properties by the states which exist across the Fermi energy level.

Interactions between the G, CB, and NBR were studied to know how the NBR matrix influences the properties of the CB-G synergy. The most stable interactions where the energy was found to be minimum are shown in Figure 5(a). The band gap of the complex increased by 44% indicating reduction in its conductivity properties. The incorporation of the CB-G into NBR insulator significantly altered the bandgap of the CB-G complex. It can be seen in the DOS (Figure 5(b)) that there are more peaks in the valence band as compared to the conduction band. The binding energy of interactions between CB-G was found to be 1203.1 ev and this value decreased to 1105.6 ev upon mixing NBR with CB-G. However, incorporating G into NBR-CB increased the binding energy to ~29%.

Interactions of CB-NT in NBR. The NT was optimized with an average C-C bond length of 1.45 angstroms. The band gap of the pristine NT was found to be 1.103 ev. The NT interacted with the CB and the most stable arrangement was found for interactions of the CB within the inner walls of the NT and is shown in Figure 6(a) with corresponding DOS, indicating that the material possessed conductive properties with a band gap of 0.983ev. Upon interactions of the complex (CB-NT) with NBR as shown in Figure 6(b), the conductivity of the material was improved by 77% with a recorded band gap value of 0.230 ev.

This sharp increase can be accounted for by the formation of several C-C bonds within the system. The DOS plot in Figure 6(b) for the NBR-CB-NT complex also revealed more states within the conduction band and high energy states across the Fermi energy level which depicts increased conductivity. There was also an increase in the binding energy from 1300.2 ev to 1566.8 ev as a result of strong intermolecular interactions. Thus, addition of NT into NBR-CB increased the binding energy to about ~81%, much better than those obtained for G interacting with NBR-CB. Thus, it was generally predicted that the synergy effect of the fillers (CB-NT, CB-G) in NBR yield better electronic and chemical interaction properties than when they are single in the NBR matrix (NBR-CB, NBR-NT, and NBR-G). The summary of the simulated findings for the single and the dual filler systems and their interactions with the NBR have been compared in the Table 2.

To further understand the theoretical predictions by the DFT approach, an experiment was set-up to examine the general properties (curing, mechanical, and electrical) of these fillers (dual or single) in presence of NBR has been discussed in the next sections. And, the best composition was selected for high deformation applications.

Curing and mechanical properties

Table 3 contains the cure characteristics at 160°C, tensile properties like strength (TS), elongation at break E_{br}(%), modulus at 100 (M100) and 300% (M300). Also, the equilibrium swelling ratio (Q_r) and crosslinking density, n_c(mol/cm^3) are reported in Table 3. Although there seem to be no any significant differences in t_{s2} among the vulcanizates, but a clear differences in t_{90} can be observed. That is, the t_{90} are higher for the composites than the gum with associated lower CRI. It is also interesting to observe that the incorporation of G or NT into NBR-CB$_H$ further reduced their cure rates than their individual vulcanizates. The NBR-CB$_H$-NT$_L$ showed the highest t_{90} and lowest CRI than the remaining compositions probably due to the poor interactions it has with the polar NBR during crosslinking reaction.[24,32,33] In particular, G contains numerous polar hydroxyl groups (C-O—H, O—C = O, O—H and C—O—C) which participate in crosslinking process and therefore delay the overall vulcanization process.[34] This phenomena is widely observed among silica filled compounds owing to their acidic nature as reported earlier by Kim and Ali groups.[33,35] Highly polar NBR-GO and NBR-G composites exhibited shorter curing time than the case of NBR-exfoliated graphite (GRT) composites due to the non-polar nature of the GRT.[34]

Despite the poor curing rates, the nanoparticles improved the viscosity (M_L) and exhibited stronger reinforcement advantage in the NBR matrix. As can be seen in Table 3, higher rheological mechanical strength (M_H) and its crosslinking density indicators (ΔM) were observed for the composites than the neat NBR. The improvement in cure rheological mechanical properties (M_H and ΔM) of the composites is also in accordance with lower equilibrium swelling ratio (Q_r), higher chemical crosslinking density n_c(mol/cm^3) and consequently higher TS (MPa) and modulus (M100 and M300)

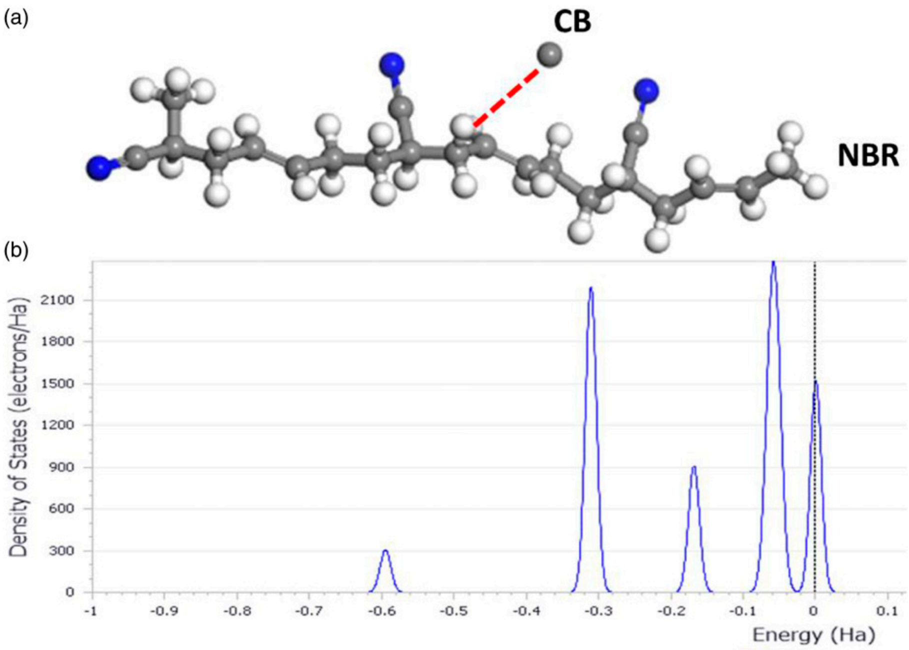

Figure 3. Showing (a) optimized NBR-CB and (d) DOS for NBR-CB interaction.

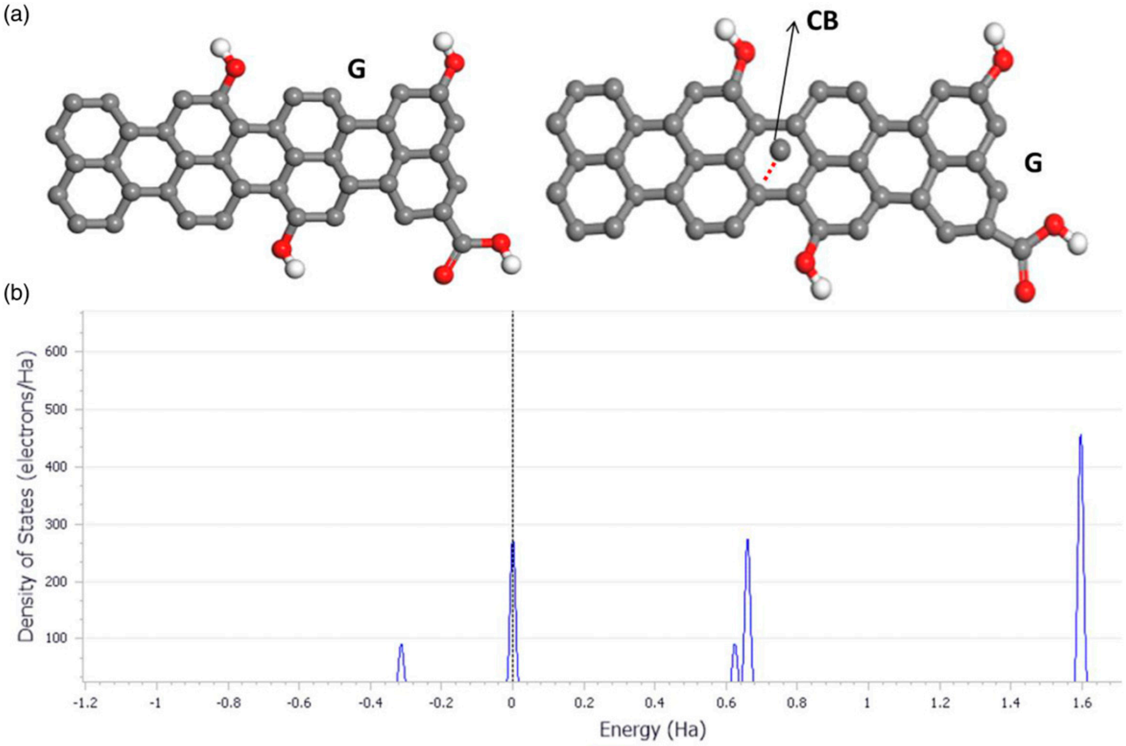

Figure 4. showing (a) optimized G and CB-G and (b) DOS plots for CB-G interaction.

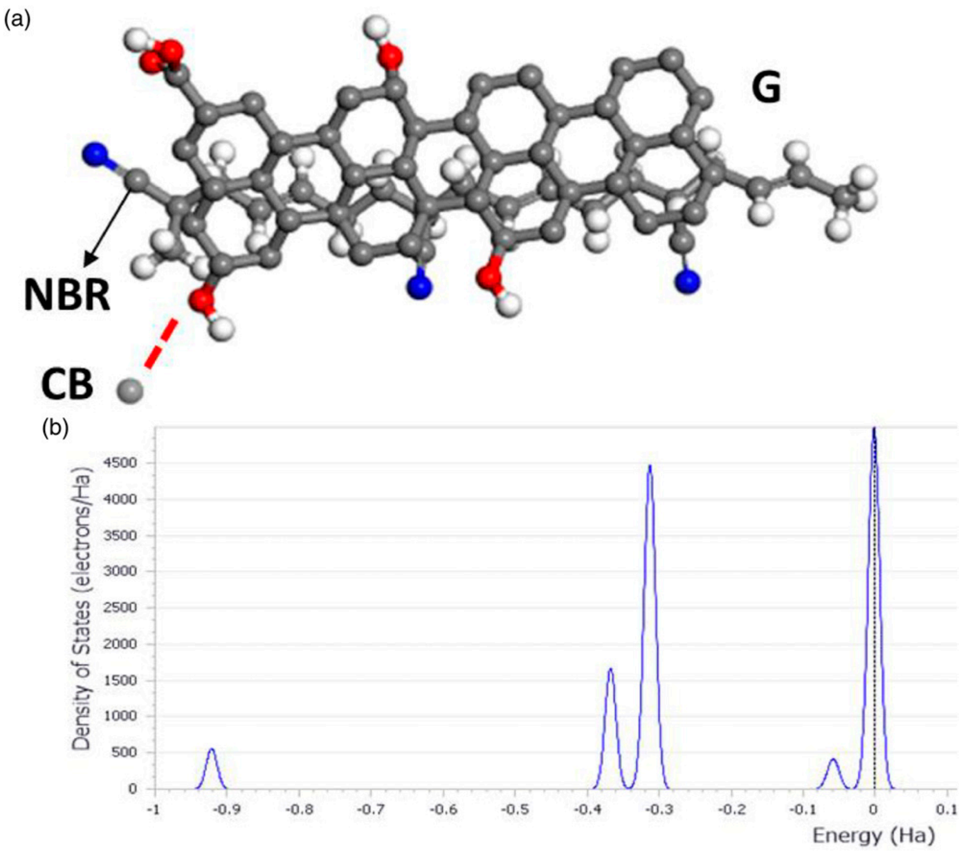

Figure 5. showing (a) optimized NBR-CB-G structure and (b) DOS for Optimized NBR-CB-G structure.

properties. The enhanced parameters are usually associated with stronger filler-polymer and filler-filler interactions.[33,35] The NBR-CB_H-G_L generally showed the highest mechanical properties (TS (MPa), E_{br}(%), M100 (MPa), M300 (MPa), and n_c(mol/cm^3)) particular when compared with the other dual filled composites (NBR-CB_H-NT_L). When the reinforcement factor, $?_f$ (M300/M100) is computed, NBR-CB_H-NT_L exhibited the highest $?_f$ leading its counterpart (NBR-CB_H-NT_L) over 22%. The enhancement may be related to the high crosslinking density and the effective complementary functionality of CB_H-G_L filler networks in NBR matrix. It was also practical for the G_L nanosheets to fill the voids in the voluminous structure of CB_H. This in effect could reduce probable voids that have tendency to act as defect sites for mechanical failure. It appears there was a poor interaction of CB_H-NT_L blends within NBR, since the TS of NBR-CB_H-NT_L declined relative to NBR-NT_H and NBR-CB_H-G_L systems. Contrary to the high intermolecular interactions in NBR-CB_H-NT_L measured by high binding energy (1566.8 ev), as predicted by DFT approach, the outer part of NT is practically proven to interact poorly with rubber molecules.[36,37] This is in regards to the previous work where it was observed that NT slipped out of the matrix of natural rubber (NR) upon straining and later reverted quickly back into the matrix after some time, reported by Nah et al.[36,37] However, NBR exhibited higher E_{br} (%) and lower modulus due to the absence of the reinforcing fillers.

Hysteresis loss study

The hysteresis studies of representative samples of NBR-CB_H, NBR-CB_H-G_L, and NBR-CB_H-NT_L area compared in Figure 7(a)–(c). Clearly, upon incorporation of G_L into NBR-CB_H, similar area under the curves due to breaking and recovering of the filler networks can be observed for NBR-CB_H and NBR-CB_H-G_L. It is interesting to observe that the trend of the curve area changed when NT_L was incorporated into NBR-CB_H (Figure 7(c)).

The area of the curve seem to have increased, this is associated with higher hysteresis loss,[38–41] presumably due to the poor NT interactions with NBR-CB_H system, since the NT generally has poor interactions with rubber matrix.[36,37] The hysteresis losses observed in this present work for the single and dual fillers systems are much lower compared to those obtained for highly filled rubber compounds intended for green tire tread design reported earlier

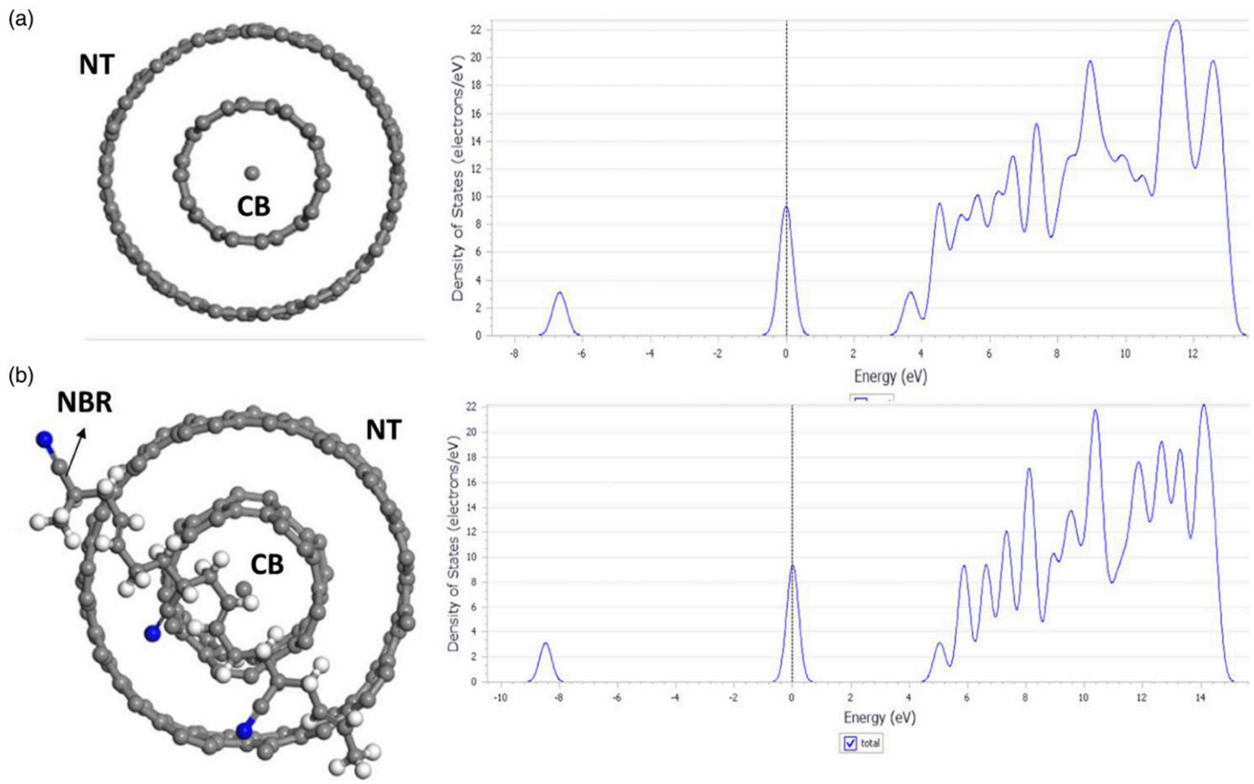

Figure 6. The (a) optimized CB-NT structure and DOS of CB-NT structure (b) optimized NBR-CB-NT and DOS for NBR-CB-NT structures.

Table 2. Electronic/binding energy properties of interacting carbon based fillers in NBR matrix.

Code/Properties	HOMO(Ev)	LUMO(Ev)	BG(Ev)	BE(Ev)
NBR	−21.965	−14.327	7.638	—
CB	−13.221	−11.241	1.98	—
PG	—	—	0.07	—
G	−16.343	−15.15	1.193	—
NT	−6.107	−5.004	1.103	—
NBR-CB	−14.029	−10.254	3.775	864.2
	Synergy effect			
CB-G	−16.327	−15.202	1.125	1203.1
NBR-CB-G	−15.385	−13.37	2.015	1105.6
CB-NT	−6.131	−5.148	0.983	1300.2
NBR-CB-NT	−17.674	−17.444	0.23	1566.8

BG: band gap (ev) and BE: binding energy (ev).

by Mensah et al.[42] However, the changes in hysteresis of the single and dual filler systems may account for the nature of filler networks (CB-CB, G-G, NT-NT, CB-NT$_L$, and CB-G$_L$) during higher deformations.

Electrical properties

Electrical resistance. The surface resistances of the unstrained nanocomposites are shown in Figure 8(a) while the resistances for the representative cross-sectioned samples are shown in Figure 8(b). It is evidenced that incorporating of the fillers single or dual into the pure NBR significantly reduced the electrical resistance from $\sim10^{13}$ to $\sim10^{6}$ Ω. The NBR-CB$_H$-G$_L$ and NBR-CB$_H$-NT$_L$ showed the lowest resistance with the NBR-NT$_L$ and NBR-G$_L$ being the highest after NBR. It is remarkable to observe that the dual filler systems (NBR-CB$_H$-G$_L$ and NBR-CB$_H$-NT$_L$) showed similar results with the theoretical predictions in the DFT modeling, although such observation was different in the single filler systems. This was expected, due to the high purity of NT than the defective G, prepared through excessive oxidation and reduction by modified Hummers method.[29,43] Unlike G, defect-free graphene sheets show higher electrical conductivity properties.[29] Thus, electrical resistance of the G$_L$ and NT$_L$ in NBR-CB$_H$ may be influenced by the shape of fillers, purity level, state of dispersions, and their interactions with CB and the NBR matrix.[24,25,32] Although slight deviations can be seen between the sheet resistance and the cross-sectioned samples (Figure 8(b)), a general trend of improvement in electrical resistance of the NBR-CB$_H$ was observed when G$_L$ was incorporated.

The results observed in Figure 8(a) and (b) is very fascinating, since most CB-filled rubber composites shows percolation threshold above 30 phr of CB loading,[20,32,44,45]

Table 3. Cure and mechanical properties of NBR filled with single and dual carbon-based fillers.

Code	M_H(dNm)	M_L(dNm)	ΔM(dNm)	t_{90} (min)	t_{S2} (min)	CRI(/min)
NBR	37.2	3.2	34.0	4.0	2.4	61.4
NBR-G_L	42.1	3.7	38.4	4.5	2.6	53.5
NBR-CB_H	43.0	6.1	36.9	6.7	2.2	22.5
NBR-CB-G_L	47.8	5.2	42.6	7.6	2.1	18.4
NBR-NT_H	39.5	4.3	35.2	6.3	2.2	24.1
NBR-CB-NT_L	38.8	3.9	34.9	11.4	2.2	10.9
		Tensile and crosslinking density properties				
Code	TS(MPa)	E_{br}(%)	M100(MPa)	M300(MPa)	Q_r	n_c(mol/cm^3)
NBR	4.3	411.3	1.8	4.3	2.24	1.4
NBR-G_L	5.8	239.2	2.7	5.8	2.12	1.5
NBR-CB_H	9.5	367.5	2.5	8.2	1.84	2.9
NBR-CB-G_L	10.0	327.8	3.1	9.5	1.75	3.1
NBR-NT_H	7.4	288.8	2.8	-	1.79	2.8
NBR-CB-NT_L	7.0	323.8	2.5	6.7	1.85	2.8

M_H: maximum torque, M_L: minimum torque, $\Delta M=(M_H-M_L)$, t_{s2}: onset of cure, t_{90}: optimum cure time, and CRI = $100/(t_{90}-t_{s2})$

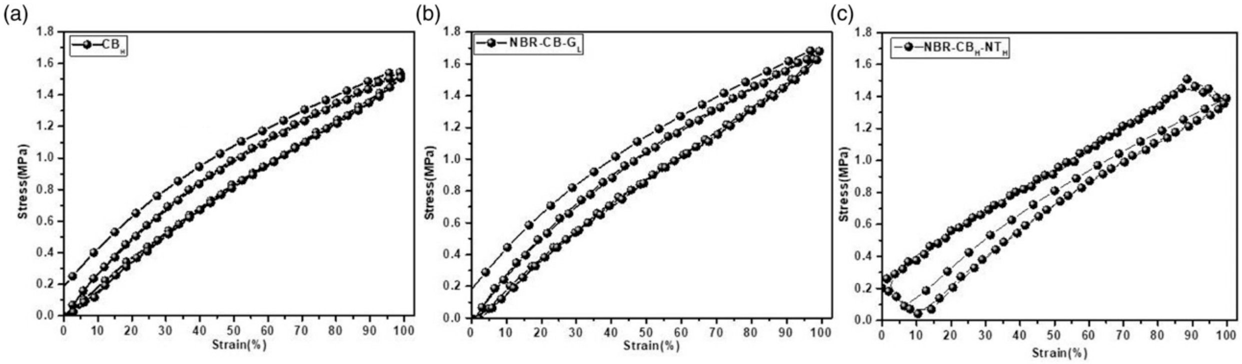

Figure 7. Measuring the hysteresis losses of representative samples; (a) NBR-CB_H, (b) NBR-CB_H-G_L and (c) NBR-CB_H-NT_L.

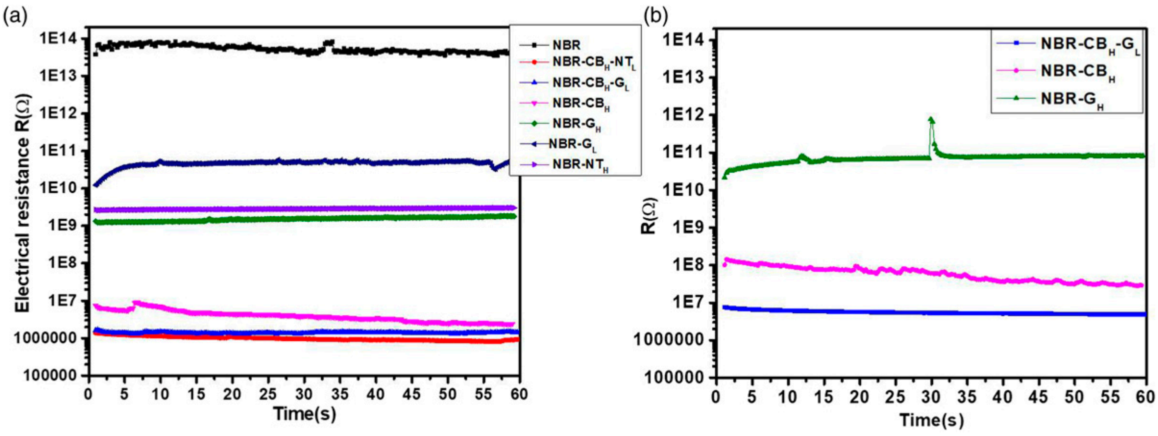

Figure 8. Electrical resistance (R) of unstrained composites; (a) is sheet resistance and (b) resistance of cross-sectioned samples.

even though low content of multiwall NT and G-systems have shown percolation threshold around ≥ ~0.5 phr in rubber but with very high electrical resistance compared to those achieved by the dual systems in the present study.[32,44,46] Incorporating (~0.1 phr of NT or G) into 5 phr of NBR-CB blend has further improved the electrical resistance from~10^7 Ω (for NBR-CB_H) to ~10^6 Ω for NBR-CB_H-G_L or NBR-CB_H-NT_L.

By comparison, the percolation threshold was obtained in this present work with lower amount of filler of 5.1 phr compared to that of epoxide Natural rubber (ENR-50) filled with different types of CB which attained percolation threshold above (10–30 phr)[45] and rubber reinforced with ≥ ~10 phr obtained for NT and G-based fillers.[32,44,46] The G_L or NT_L could interconnect to fill the pores left within the known CB-CB network structures. This therefore may increase the chances of formation and increasing the number of conductive path within NBR-CB_H-G_L and NBR-CB_H-NT_L composites systems, as depicted in Figure 9(a)–(c).

Effect of strain on electrical resistance. As for strain sensors, the linearity or nonlinear (exponential) profile between resistance and strain is desired.[1–5] Quite complicated results were reported in this regard for rubber-like composites containing the conducting particles.[1–3]

Generally, the resistance of rubber composites containing spherical particles like carbon blacks (CB) increases at relatively lower strain region and it decreases with further straining to higher level below Payne effect [41,47] due to the action of breaking of the filler-filler network, which acts as the conducting path. The latter decrease in resistance is attributed to the recombination of neighboring particles due to contraction in the directions of width and thickness. Herein, this trend may also be applicable for conducting fillers like NT and G but could be different for their synergies (CB-NT and CB-G). On straining, the electrical resistance of NBR-CB_H increased exponentially but at lower strain level (~30%), as higher strain level lowers resistances. But upon incorporating of G_L, the exponential growth continued to higher levels. To check the sensing behavior of the compounds, the GF values given in equation[1] were calculated from the slopes between $\Delta R/R_o$ and strain (ε) of the various composites. A representative plot is shown in Figure 10(a)–(c) for the case of NBR-G_H, NBR-CB_H, and NBR-CB_H-G_L, respectively. All the composites generally exhibited a linear relationship at strain levels of 5–40% with high regression coefficient (r^2~0.95), except NBR-CB_H and NBR-CB_H-G_L composites which exhibited exponential behavior. Thus, the GF values were in the range of ~3.5, ~10^4, and ~10^5 for NBR-G_H, the NBR-CB_H, and NBR-CB_H-G_L, respectively (Figure 10(a)–(c)).

The NBR-CB_H (Figure 10(b)) showed higher GF than that NT-containing samples and the samples containing only G (NBR-G_L and NBR-G_L). Figure 11(a)–(f) is presented to explain the mechanism leading to the exponential growth in resistance for the dual filler systems as a function of strain. Blending of small amount (0.1 phr) of NT or G into NBR-

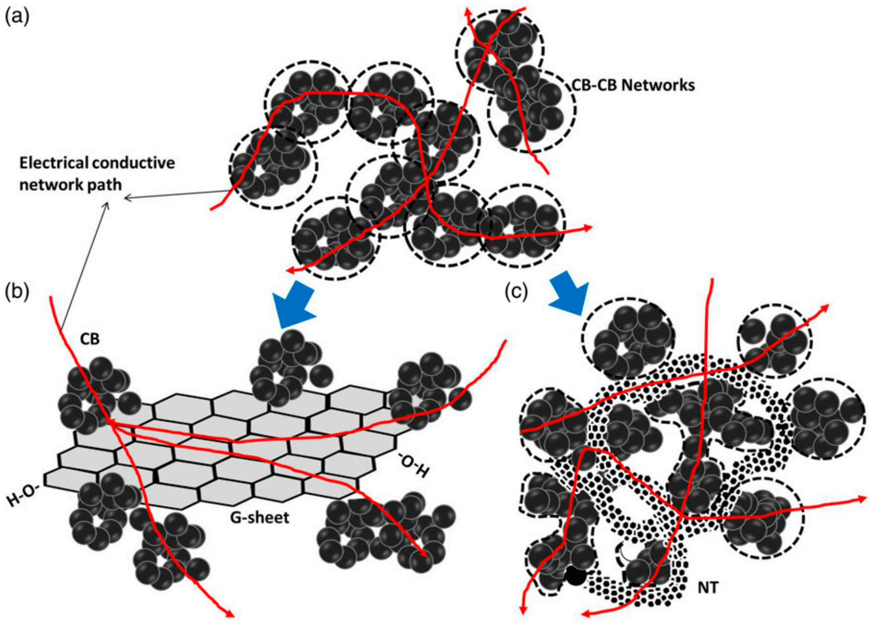

Figure 9. Proposed mechanism to create a continuous electrical conductive network within (a) carbon black (CB) using (b) G and (c) NT sheets.

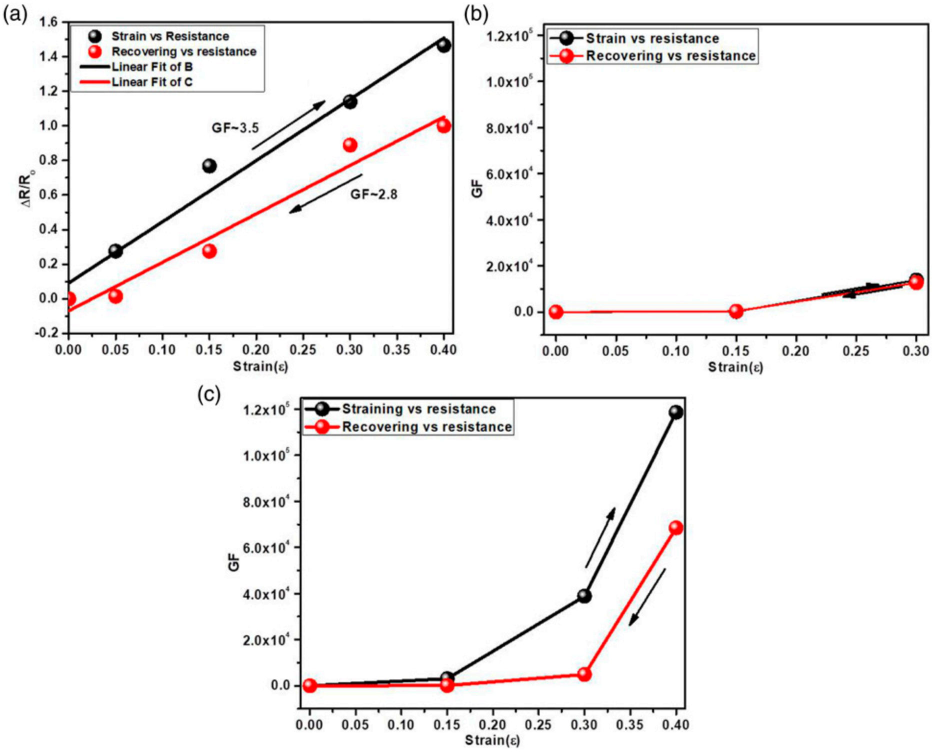

Figure 10. The GF of representative sensors during deformation and relaxation; (a) NBR-G_H, (b) NBR-CB_H, and (c) NBR-CB_H-G_L.

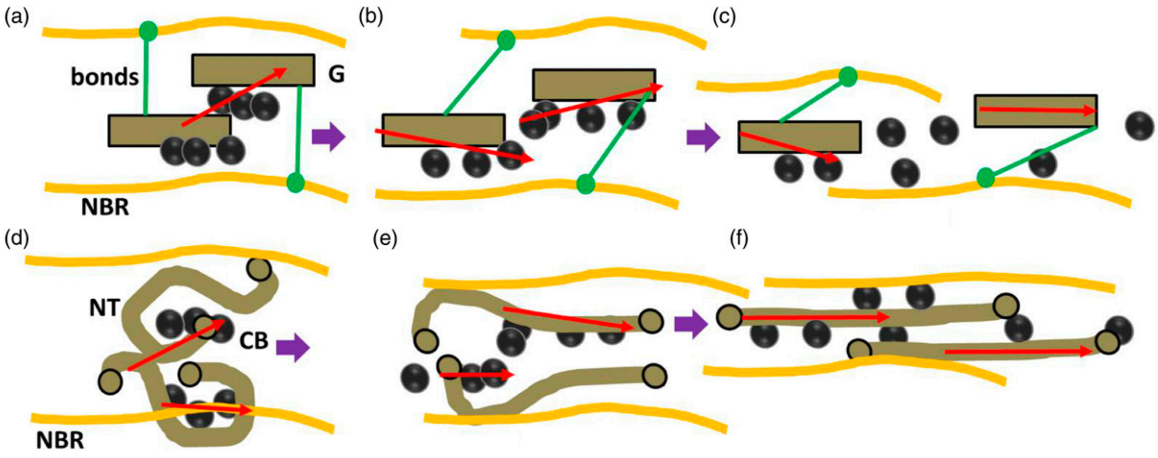

Figure 11. an illustration of the effect of uniaxial strain on electrical conductivity mechanism of dual fillers like NT-CB and CB-G in the presence of NBR matrix.

CB_H initially improved the electrical conductivity when unstrained. However, the NBR-CB_H-G_L seems to show faster electrical reaction as a function of uniaxial strain than the rest. The strong interactions of NBR-G and CB-G due to bonds like NBR—G—S_x—G—NBR and hydrogen bonds NBR or CB—C≡N—OH—G tightens up the structures (NBR-G and CB-G). However, attempt to strain the tight bonds in NBR-G could easily destroy the weak polar interactions in G-CB, leading to breaking of conductive network path within the bulk structure (NBR-CB_H-G_L). Higher strains resulted in higher breakdown of G-CB networks (with higher electrical resistances). The filler-filler break-down is a common phenomenon observed in Payne effect for rubber-filler composites.[41,48] Hence, by this mechanism an increase in strain further increased the resistances in NBR-CB_H-G_L to exponential levels. However, in case of the coiled NT which is poorly bonded to the matrix[36,37] and the CB, uniaxial strain could easily enable the

Table 4. Comparison of GF of various polymer-based sensing materials/devices over the years.

Composites/Sensing elements	Strain (%)	GF	References	Remarks
NBR-CB/G$_L$(Tensile)	40	$\sim 1.2 \times 10^5$	Present work	2022
NBR-CB(Tensile)	30	$\sim 10^4$	Present work	2022
Pristine graphene on flexible PDMS	—	$>5 \times 10^3$	Na et al.[50]	2022
PDMS-CB-G	28–44	1.9×10^4	Song et al.[18]	2021
PDMS-LIG[x] graphene	0–31.8	37.8	Huang et al.[51]	2020
EPDM-graphene	0–68	~38	Qiu et al. [16]	2020
NR-pristine graphene	—	46	Liu et al.[8]	2019
G-on-rubber substrate	25	6–35	Liu et al. [52]	2016
Epoxy Polymer-G (Tensile mode)	0.003	12.8	Tung et al.[15]	2016
P(VDF-TrFE)[a] fiber/ZnO nanowire	30	4.59	Shuai et al.[11]	2016
Epoxy-NT-modified fiber	0.40	1.9–4.0	Hongbo et al.[9]	2015
PDMS-NT Ecoflex	510	0.61	Amjadi et al.[53]	2015
NR-G	800	35	Boland et al.[14]	2014
NR-GRT sensors (Tensile mode)	50–246	23.7–346.6	Tadakaluru et al.[13]	2014
NR-NT sensors (Tensile mode)	100–620	5.5–43.4	Tadakaluru et al.[13]	2014
Flexible GRT-on-paper based sensor	—	0.84[b]	Ren et al.[54]	2012
Flexible GRT-on-paper based sensor	—	0.90[b]	Liu et al.[55]	2011
Polymer-NT	280	0.06~0.82	Yamada et al.[12]	2011
Epoxy Polymer-NT (Tensile mode)	—	117	Hu et al.[10]	2010
Epoxy Polymer-NT (Tensile mode)	—	62	Hu et al.[10]	2010
PVA-PSF*-NT	—	0.208	Loh et al.[3]	2008

P(VDF-TrFE)[a]. Poly(vinylidene fluoride–trifluoro-ethylene)*. PSF: (poly(sodium 4-styrene-sulfonate), and[b] Sensitivity measured in (mV/mN)Laser-induced graphene (LIG)[x]

NT to regain their tubular structures while sliding and rolling roll over the CB networks to constitutes and to maintain the high electrical conductivity levels. Consequently, by this mechanism, unloading of the stress led to inability of the CB, CB$_H$-G$_L$, or CB$_H$-NT$_L$ particles to recover their original arrangements within the relaxed NBR matrix due to hysteresis loses. However, in view of GF, the NBR-CB$_H$-G$_L$ was the best candidate for strain sensor allocations with high mechanical properties guarantee. To the best of our knowledge, the obtained GF value for NBR-CB$_H$-G$_L$ (1.2×10^5) obtained at 40% has not been reported so far. When the GF value of ~2 for metallic strain sensors are considered,[3,12,49] the NBR-CB$_H$-G$_L$ composite materials has exhibited high performances. The obtained GF for the present work have been compared in Table 4, along with various other polymer-based sensors reported over the years.

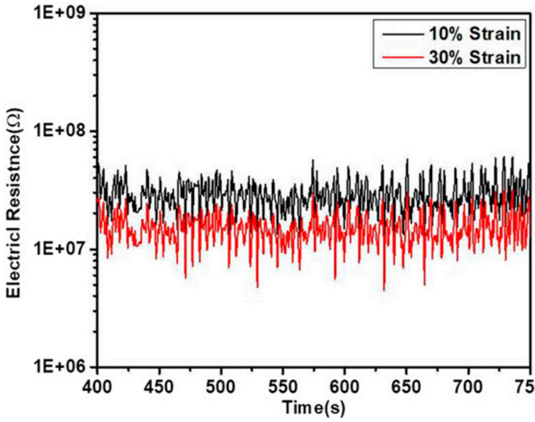

Figure 12. Electrical resistance during dynamic straining condition for NBR-CB$_H$-G$_L$ composite.

Effect of dynamic strain on electrical resistance. For applications as strain sensors, the materials should maintain the electrical stability and bear the dynamic deformation at given strains. For checking the dynamic sensitivity of the best candidate of NBR-CB$_H$-G$_L$, the electrical resistance was monitored at 10 and 30% strains, after preconditioning for 400 s to stabilize the sample from any effect like Mullin's effect,[56] as shown in Figure 12.

The change in electrical resistance seems quite stable for the two strain levels maintained at $\sim 10^7 \Omega$ from the unstrained state (MΩ). The current observation is comparable to those achieved for NR-NT sensor by Tadakaluru et al.,[13] PDMS-Laser-induced graphene (LIG) sensor by Huang et al.,[51] and that of EPDM-graphene sensor by Qiu et al.[16]

Applications

Sounds and breath sensing. The response of a sensor based on NBR-CB$_H$-G$_L$ for monitoring speech and breathing patterns (normal and fast) have been compared in Figure 13(a) and (b), respectively. Figure 13(a) is a plot of signals with different deformations from the throat of a male subject. It includes NB: normal breathing, SD: whooo sound, and speech (S: "my name is Bismark"). The differences in electrical resistance among NB, SD, and S are clearly labeled.

According to Palazzolo.[57] The human throat experiences small-scaled vibrations in the vocal fold (chord). The left and right fold constitutes a "V" shape when viewed from above, the folds are pulled apart when breathing and pulled together during speech. This kind of mechanisms echoes frequencies with corresponding small deformations which can be measured and interpreted. As seen SD and S sounds have similar higher electrical resistance profile compared to the NB probably due to higher deformations (vibrations) generated. In Figure 13(b), the difference between normal breathing (NB: black color) and fast breathing (FB: red-color) from are clearly distinguishable from their resistance patterns. The FB showed higher electrical resistance response ($\sim10^{12}$ Ω.cm) compared to the NB ($\sim10^{8}$ Ω.cm), this is due to the high deformation received by the throat as tiny vibrations are rapidly co-ordinated from the heartbeat.[57] At the same time, some fluctuations are observed in all cases and this may probably due to due the interference of the heartbeat during breathing. The current breathing rhythm appears as "zig-zag" waveforms, which is different from the work of Boland et al.,[14] where a Fourier transform

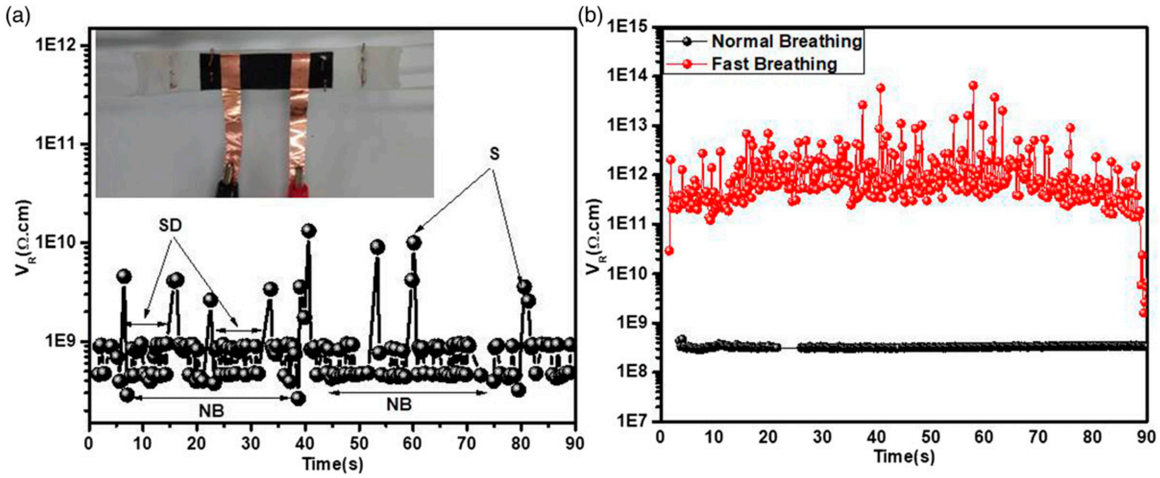

Figure 13. Application of NBR-CB$_H$-G$_L$ for (a) detecting electrical resistance responses from the throat and (b) monitoring human breathing patterns.

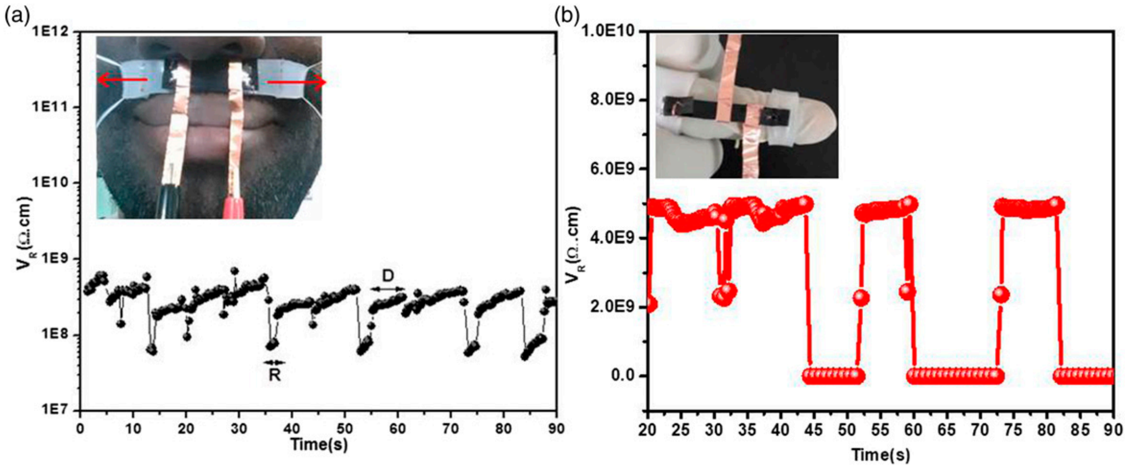

Figure 14. Sensing behavior of NBR-CB$_H$-G$_L$ sensor; (a) bending and relaxation of the finger and (b) deformation (smiling) and relaxation of the face for sensor placed in-between the mouth and the nose.

component associated with breathing was detected. NR-pristine graphene sensor was developed and used to detect subtle motions such as breathing or heartbeat by Liu et al.[8] However, the reported sensing performance (GF~46) was lower compared to those obtained for NBR-CB_H-G_L sensor in this present work.

Facial and finger deformation sensing. The results obtained by the NBR-CB_H-G_L sensor placed in-between the mouth and the nostril is shown in Figure 14(a). The deformation (D) represent happy/smiling mood and relaxation (R) shows the unhappy/non-smiling mood. The D in Figure 14 resulted in ~6% strain in addition to the pre-strain condition (~1%). The electrical signal passed through a lower (R) to medium (beginning of D) and higher state (D) with differences in resistances. This depicts the fast response of the sensor (NBR-CB_H-G_L) for detecting even little deformations/vibrations from the human body and motion. The bending (bending angle of ~75°) and the relaxation (0° angle) of the second finger were tested and the pattern is as shown in Figure 14(b). The electrical resistance profiles for the fingers showed a kind perfect square wave behavior. The bending generally resulted in higher deformation corresponding to higher electrical resistance response than the relaxation process. A similar waveform was earlier reported by Amjadi et al.[53] and recently by Na et al.[50] who recorded a gauge factor above 5000 for graphene on flexible substrate.

By considering the cost of producing vertical graphene on flexible PDMS, the current design though simple but with high GF ~10^5 than those reported. Therefore, the NBR-CB_H-G_L sensor has demonstrated the ability to detect signals coming from deformed human fingers with repeatability, stability and could possibly do same for wrist and the knee.

Conclusions

The interactions and the electronic properties among carbon based fillers NT, CB, G and their synergy effect were studied in the presence of acrylonitrile butadiene rubber (NBR) by using DFT modeling approach. It was observed that incorporating these conductive fillers into NBR, improved the binding and electrical conductivity properties, with the dual filler been the best. To verify the theoretical predictions, an experiment was set-up, and the various composites of NBR filled with fillers such as G, NT, CB and their synergy (NBR-CB_H-G_L and NBR-CB_H-NT_L) compositions were prepared via a combination of conventional solution and solid processing techniques. The DFT predictions were generally in correspondence with the experimental results. The optimum design (NBR-CB_H-G_L) was found to show high tensile strength, crosslink density, and improved electrical properties. On account of strain sensing performance, NBR-CB_H-G_L exhibited good stability of filler networks measured by low hysteresis loss and exponential relationship of strain-resistance, demonstrating high GF~10^5 which is ~900% development of NBR-CB_H composite (GF ~10^4). This was explained by the mechanical disruptions caused by tight NBR-G structures which in turn break CB networks on straining, leading to exponential growth in electrical resistance. The NBR-CB_H-G_L also demonstrated relatively good stability and repeatability in electrical resistance response for the cyclic load sensing. In terms of applications, NBR-CB_H-G_L sensors exhibited the capability to be used as a simple sensitive wearable sensor for detecting human bodily motions like human speeches, sounds, facial deformations, bending and relaxation of the fingers. Therefore, the current work provides a simple route of controlling the microstructure of viscoelastic rubber matrix with small amount of carbon based fillers like NT or G into conductive CB for harvesting high GF, intended for advanced sensor applications involving vibrations and deformations.

Acknowledgements

We acknowledge the assistant offered by Prof. Changwoon Nah of JBNU (South Korea) for granting the chance to use their facilities for this work is acknowledged. The University of Ghana – Carnegie Next Generation of African Academics (UG-Carnegie NGAA) Project and the Office of Research Innovation and Development (ORID) at the University of Ghana toward the completion of the manuscript.

Declaration of Conflicting Interests

The author(s) declared no potential conflicts of interest with respect to the research, authorship, and/or publication of this article.

Funding

The author(s) received no financial support for the research, authorship, and/or publication of this article.

Data Availability Statement

The data used to support the findings of this study are available from the corresponding author upon request.

ORCID iDs

Bismark Mensah https://orcid.org/0000-0001-9098-1110
Clive Dompreh https://orcid.org/0000-0003-1594-7398

References

1. Yin G, Hu N, Karube Y, et al. A carbon nanotube/polymer strain sensor with linear and anti-symmetric piezoresistivity. *J Compos Mater* 2011; 45(12): 1315–1323.
2. Xu W and Allen MG. Fabrication of patterned carbon nanotube (CNT)/elastomer bilayer material and its utilization as force sensors, In Allen MG (eds). Solid-State Sensors, Actuators and Microsystems Conference. Denver, CO, 21-25, June 2009.
3. Loh KJ, Lynch JP, Shim BS, et al. Tailoring piezoresistive sensitivity of multilayer carbon nanotube composite strain sensors. *J Intell Mater Syst Structures* 2008; 19(7): 747–764.
4. Luheng W, Tianhuai D and Peng W. Influence of carbon black concentration on piezoresistivity for carbon-black-

filled silicone rubber composite. *Carbon* 2009; 47(14): 3151–3157.

5. Wang L, Ma F, Shi Q, et al. Study on compressive resistance creep and recovery of flexible pressure sensitive material based on carbon black filled silicone rubber composite. *Sensors Actuators A: Phys* 2011; 165(2): 207–215.
6. Zhou B, Li C, Liu Z, et al. A highly sensitive and flexible strain sensor based on dopamine-modified electrospun styrene-ethylene-butylene-styrene block copolymer yarns and multi walled carbon nanotubes. *Polymers (Basel)* 2022; 14(15): 11.
7. Garcia JR, O'Suilleabhain D, Kaur H, et al. A simple model relating gauge factor to filler loading in nanocomposite strain sensors. *ACS Appl Nano Mater* 2021; 4(3): 2876–2886.
8. Liu H, Gao H and Hu G. Highly sensitive natural rubber/pristine graphene strain sensor prepared by a simple method. *Composites B: Eng* 2019; 171: 138–145.
9. Dai H, Thostenson ET and Schumacher T. Processing and characterization of a novel distributed strain sensor using carbon nanotube-based nonwoven composites. *Sensors* 2015; 15(7): 17728–17747.
10. Hu N, Karube Y, Arai M, et al. Investigation on sensitivity of a polymer/carbon nanotube composite strain sensor. *Carbon* 2010; 48(3): 680–687.
11. Shuai Chen ZL, Chen D, Chen Z, et al. Highly flexible strain sensor based on ZnO nanowires and P(VDF-TrFE) fibers for wearable electronic device. *Sci China Mater* 2016; 59.
12. Yamada T, Hayamizu Y, Yamamoto Y, et al. A stretchable carbon nanotube strain sensor for human-motion detection. *Nat Nano* 2011; 6(5): 296–301.
13. Tadakaluru S, Thongsuwan W and Singjai P. Stretchable and flexible high-strain sensors made using carbon nanotubes and graphite films on natural rubber. *Sensors* 2014; 14(1): 868–876.
14. Boland CS, Khan U, Backes C, et al. Sensitive, high-strain, high-rate bodily motion sensors based on graphene-rubber composites. *ACS Nano* 2014; 8(9): 8819–8830.
15. Tung TT, Karunagaran R, Tran DNH, et al. Engineering of graphene/epoxy nanocomposites with improved distribution of graphene nanosheets for advanced piezo-resistive mechanical sensing. *J Mater Chem C* 2016; 4(16): 3422–3430.
16. Qiu A, Aakyiir M, Wang R, et al. Stretchable and calibratable graphene sensors for accurate strain measurement. *Mater Adv* 2020; 1(2): 235–243.
17. Kurian A, Mohan VB and Bhattacharyya D. Embedded large strain sensors with graphene-carbon black-silicone rubber composites. *Sensors Actuators A Phys* 2018; 282: 11.
18. Song P, Wang G and Zhang Y. Preparation and performance of graphene/carbon black silicone rubber composites used for highly sensitive and flexible strain sensors. *Sensors Actuators A: Phys* 2021; 323: 112659.
19. Cai W, Huang Y, Wang D, et al. Piezoresistive behavior of graphene nanoplatelets/carbon black/silicone rubber nanocomposite. *J Appl Polym Sci* 2014; 131(3): 11.
20. Song P, Song J and Zhang Y. Stretchable conductor based on carbon nanotube/carbon black silicone rubber nanocomposites with highly mechanical, electrical properties and strain sensitivity. *Composites Part B: Eng* 2020; 191: 107979.
21. Cataldo F, Ursini O and Angelini G. MWCNTs elastomer nanocomposite, part 1: the addition of MWCNTs to a natural rubber-based carbon black-filled rubber compound. *Fullerenes, Nanotubes and Carbon Nanostructures* 2009; 17(1): 38–54.
22. Walter P, Podsiadły B, Zych M, et al. CNT/graphite/SBS conductive fibers for strain sensing in wearable telerehabilitation devices. *Sensors* 2022; 22(3): 800.
23. Zhu W-B, Xue S-S, Zhang H, et al. Direct ink writing of a graphene/CNT/silicone composite strain sensor with a near-zero temperature coefficient of resistance. *J Mater Chem C* 2022; 10(21): 8226–8233.
24. Mensah B, Kumar D, Lim D-K, et al. Preparation and properties of acrylonitrile–butadiene rubber–graphene nanocomposites. *J Appl Polym Sci* 2015; 132(36): 11.
25. Mensah B, Kim S, Arepalli S, et al. A study of graphene oxide-reinforced rubber nanocomposite. *J Appl Polym Sci* 2014; 131(16): 11.
26. Flory PJ and Rehner J. Statistical mechanics of cross-linked polymer networks II. *Swelling J Chem Phys* 1943; 11(11): 521–526.
27. Bristow GM and Watson WF. Cohesive energy densities of polymers. Part 1.-cohesive energy densities of rubbers by swelling measurements. *Trans Faraday Soc* 1958; 54(0): 1731–1741.
28. Najitha S and Predeep P. Electrical and optical properties of nitrile rubber modified by ion implantation. *AIP Conf Proc* 2014; 1620: 11.
29. Abid SP, Islam SS, Mishra P, et al. Reduced graphene oxide (rGO) based wideband optical sensor and the role of temperature, defect states and quantum efficiency. *Scientific Reports* 2018; 8(1): 3537.
30. Brodie BC. On the atomic weight of graphite. *Philos Trans R Soc Lond* 1859; 149: 249–259.
31. Blake P, Hill EW, Castro Neto AH, et al. Making graphene visible. *Appl Phys Lett* 2007; 91(6): 11.
32. Mensah B, Kim HG, Lee J-H, et al. Carbon nanotube-reinforced elastomeric nanocomposites: a review. *Int J Smart Nano Mater* 2015; 6(4): 211–238.
33. Kim S-M and Kim K-J. Effects of accelerators on the vulcanization properties of silica vs. carbon black filled natural rubber compounds. *Polym Korea* 2013; 37(3): 269–275.
34. Mensah B, Gupta KC, Kang G, et al. A comparative study on vulcanization behavior of acrylonitrile-butadiene rubber reinforced with graphene oxide and reduced graphene oxide as fillers. *Polym Test* 2019; 76: 127–137.
35. Ali M, Chugh JP and Haghighat S. Effects of silica on the cure properties of some compounds of styrene-butadiene rubber. *Iranian Polym J* 2000; 9(2): 1026–1265.
36. Nah C, Lim JY, Sengupta R, et al. Slipping of carbon nanotubes in a rubber matrix. *Polym Int* 2011; 60(1): 42–44.
37. Nah C, Lim JY, Cho BH, et al. Reinforcing rubber with carbon nanotubes. *J Appl Polym Sci* 2010; 118.
38. Fröhlich J, Niedermeier W and Luginsland HD. The effect of filler–filler and filler–elastomer interaction on rubber reinforcement. *Composites A: Appl Sci Manufacturing* 2005; 36(4): 449–460.
39. Kucherskii AM. Hysteresis losses in carbon-black-filled rubbers under small and large elongations. *Polym Test* 2005; 24(6): 733–738.
40. D'Ambrosio P, De Tommasi D, Ferri D, et al. A phenomenological model for healing and hysteresis in rubber-like materials. *Int J Eng Sci* 2008; 46(4): 293–305.

41. Li Z-Y, Song Y-H and Zheng Q. Payne effect and weak overshoot in rubber nanocomposites. *Chin J Polym Sci* 2022; 40(1): 85–92.
42. Mensah B, Agyei-Tuffour B, Nyankson E, et al. Preparation and characterization of rubber blends for industrial tire tread fabrication. *Int J Polym Sci* 2018; 2018: 2473286.
43. Shahriary L and Athawale A. Graphene oxide synthesized by using modified hummers approach. *Int J Renew Energ Environ Eng* 2014; 02(01): 11.
44. Mensah B, Gupta KC, Kim H, et al. Graphene-reinforced elastomeric nanocomposites: A review. *Polym Test* 2018; 68: 160–184.
45. Salaeh S, Boiteux G, Cassagnau P, et al. Conductive elastomer composites with low percolation threshold based on carbon black and epoxidized natural rubber. *Polym Composites* 2018; 39(6): 1835–1844.
46. Das A, Kasaliwal GR, Jurk R, et al. Rubber composites based on graphene nanoplatelets, expanded graphite, carbon nanotubes and their combination: a comparative study. *Composites Sci Tech* 2012; 72(16): 1961–1967.
47. Yamaguchi K, JJC B and Thomas AG. Electrical and mechanical behavior of filled elastomers. I. The effect of strain. *J Polym Sci B: Polym Phys* 2003; 41(17): 2079–2089.
48. Hayichelaeh C, Reuvekamp LAEM, Dierkes WK, et al. Reinforcement of natural rubber by silica/silane in dependence of different amine types. *Rubber Chem Tech* 2017; 90(4): 651–666.
49. Luhrs CC, Daskam CD, Gonzalez E, et al. Fabrication of a low density carbon fiber foam and its characterization as a strain gauge. *Materials* 2014; 7(5): 3699–3714.
50. Na HR, Lee HJ, Jeon JH, et al. Vertical graphene on flexible substrate, overcoming limits of crack-based resistive strain sensors. *Npj Flexible Electro* 2022; 6(1): 2.
51. Huang L, Wang H, Wu P, et al. Wearable flexible strain sensor based on three-dimensional wavy laser-induced graphene and silicone rubber. *Sensors* 2020; 20(15): 4266.
52. Liu Y, Zhang D, Wang K, et al. A novel strain sensor based on graphene composite films with layered structure. *Composites Part A: Appl Sci Manufacturing* 2016; 80: 95–103.
53. Amjadi M, Yoon YJ and Park I. Ultra-stretchable and skin-mountable strain sensors using carbon nanotubes? Ecoflex nanocomposites. *Nanotechnology* 2015; 26(37): 375501.
54. Ren T-L, Tian H, Xie D, et al. Flexible graphite-on-paper piezoresistive sensors. *Sensors* 2012; 12(5): 6685–6694.
55. Liu X, Mwangi M, Li X, et al. Paper-based piezoresistive MEMS sensors. *Lab A Chip* 2011; 11(13): 2189–2196.
56. Mullins L. Softening of rubber by deformation. *Rubber Chemistry Technology* 1969; 42(1): 339–362.
57. Palazzolo A. *Vibration theory and applications with finite elements and active vibration control*. Wiley, 2016.